Theoretical description of Capillary Bridge formation in CMK-3

Lukas Ludescher[1]

[1] *Institute of Physics, Montanuniversitat Leoben, Franz-Josef Strasse 18, Leoben, 8700, Austria,*

(Dated: March 16, 2018)

In this work I aim to implement a macroscopic thermodynamic model based on Variational Principles for the description of sorption and capillary bridge formation in nanoporous carbon. The result is consistent with descriptions from surface science and is used to build a phase diagram for Nitrogen adsorption in Carbon. Also, a Python module was developed, which will be used in further works involving sorption in CMK-3 and CMK-3 type materials.

I. INTRODUCTION

Sorption in meso- and microporous materials and the deformation governing it have been studied for around one hundred years [1]. One of the key pieces of information to get the adsorption induced stress and strain in a porous material is the amount adsorbed as a function of the relative pressure [2]. When the loading and consequently the geometric arrangement of the adsorbed fluid is known, the induced stress can be calculated [2]. These concepts have only really taken off when novel synthesis techniques achieved the production of highly ordered pore systems [3] [4] few years ago. The study of the physics involved then was eased by the known pore geometry, which further led to theoretical concepts using macroscopic thermodynamics [5] or atomistic descriptions [6] [7] characterizing the sorption process. In this work we will investigate the variational concept in sorption introduced by Dobbs and Yeomans [8] in the early 1990ties using macroscopic thermodynamics and apply it to the example of highly ordered nanoporous carbon materials like CMK-3 [3] [4]. This will give us the possibility to not only develop a clear physical picture on the process of sorption in CMK-3 type materials, but will also allow for further studies involving calculations of stress [2][9][10] [11] or the evaluation of so called apparent strains in scattering experiments [12].

The geometry on the mesopouros length scale is built up from cylindrical Carbon rods on a hexagonal 2D lattice with rod istance D of roughly 10 nm, see figure 1. In adsorption, CMK-3 samples show two pronounced steps indicating two seperate capillary condensation events(Figure 2 b). This is beyond the concepts of the radially isotropic theoretical descriptions for cylindrical pores, which were developed in the 1970ties [5] and first applied to materials exhibiting cylindrical mesorpore [13] in the early 1990ties and could point to a unique behaviour in ad- and desorption. First attempts at describing the capillary condensation were carried out by J.R. Phillip [14] in the seventies of the last century, which were further investigated by Morishige [15] a decade ago. Although a theoretical framework for solving the problem of capillary condensation in these open void spaces was developed, all of these attempts fail to distinctly describe the transition from the so called 'bridged' phase to the completely filled void space.

Nowadays meso- and microporous materials are mainly investigated using computational methods such as Monte-Carlo simulations or ab-initio based methods like non-local density functional theory [6] (NLDFT) and quenched solid state density functional theory [7](QSDFT). Gor et al. [16] applied the QSDFT to CMK-3 using a cylindrical form factor to describe the open void spaces in this material. For the desorption and adsorption branch different results for the pore size distribution are obtained, which points to a not fully complete description by this simplification, although the mean pore size obtained matches earlier investigations using more basic evaluations [16] [4].

Monte-Carlo methods allow for the description of more complex geometries by using atomistic models [17], but realistically it is very hard to properly describe the actual surface chemistry well with purely theoretical interaction parameters due to the usually not well understood properties of the pore surface. In one recent study by Yelpo et al in 2017 [18], kernels for a range of pore sizes were calculated for CMK-3, describing potential of the Carbon rods by Lennard-Jones porential, which show again similar results for the pore size distribution when compared to the study carried out by Gor [16]. Another study by Jain et.al. [17] described the whole system atomistically, not replacing the carbon rods by a potential but by an assembly of carbon atoms. Then, sorption of argon was simulated in this all-atom description, showing that interconnections between the carbon rods seem to influence the sorption behaviour decisively.

All these theoretical investigations into the sorption behaviour of CMK-3 materials are either not entirely representative of the geometry in the case of ab-initio methods or are purely based on theoretical parameters, which might not be fully indicative of the real surface. Also, it is computationally expensive to conduct Monte-Carlo and ab-initio based simulations, whereas any modern desktop personal computer is able to swiftly solve the ordinary differential equations retrieved from variational methods.

This is why macroscopic thermodynamic models with individually fitted interaction parameters pose an attractive alternative [9] [11], although they don't describe pores with dimensions below two to three nanometers accurately. Consequently, we cannot offer precise quantitative interpretation of sorption isotherms, but aim to deliver a more realistic and swift description of the sorption process in CMK-3 and CMK-3 type materials.

This work will be structured the following way: First we will introduce the material and the experimental techniques in the Methods and Materials sections. Further we will shortly introduce the evaluation of rod sizes in CMK-3 materials using Small Angle X-Ray Scattering and introduce the Variational Principle for sorption in CMK-3 Materials. In the Results section we will then present the experimental results and then compare and discuss them in the Discussion part of this work.

The experimental work presented here was done at the home university (Montanuniversitt Leoben, MUL), while the theoretical model was developed, setup and tested at the host university (New Jersey Institute of Technology, NJIT).

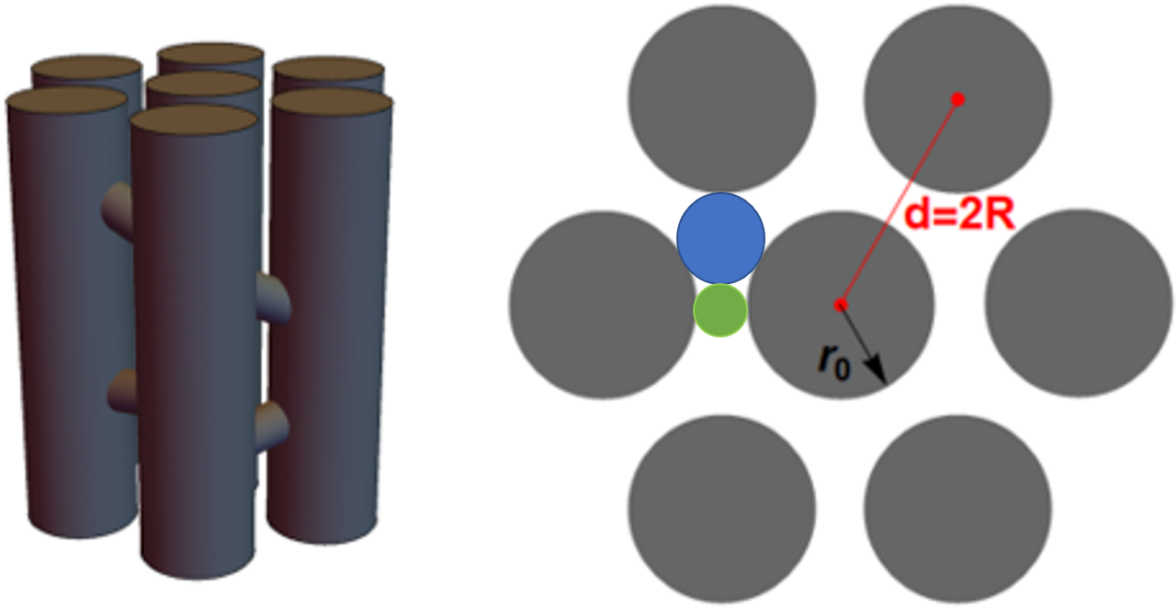

FIG. 1. Left: Topview a selection of the hexagonally ordered rods. r_0 is the mean rod diameter, $D = 2R$ is the mean distance between two rods. The blue disk shows the largest inscribed circle in the pore space, the green disk the smallest inscribed circle possible. Right:Cartoon of a selected bundle of rods in sideview. The connections between the rods are of high importance structurally. The length of the rods shown is not indicative of their true dimension.

II. METHODS AND MATERIALS

A. Materials

The material investigated in this study is CMK-3, industrial grade bought from Sigma-Aldrich. CMK-3 materials are essentially synthesised by hard templating. This process involves two stages, with the first one involving the production of a negative of the eventual carbon structure from silica and the subsequent filling with carbon and removal of the silica. Details on the synthesis are given in Ref.[4]. Because the structural details are important for the theoretical and computational details in this work, we will describe it in more detail.

Generally, three different types of pores are distinguished in porous materials [19]. Macropores are void with sizes of 50 nm and upwards, whereas micropores are defined to be smaller than 2 nm in their smallest dimension. Any void space with its smallest dimension being between 2 and 50 nm is considered a mesopore. On the mesoporous level, CMK-3 exhibits hexagonally ordered carbon nanowires with a diameter in the range of 3 to 4.5 nm and a nearest neighbour distance of about 10 to 11 nanometers. It is assumed that these nanowires are interconnected by thin strut-like structures that give stability to the hexagonal arrangement[3]. Proof of this is the total absence of hexagonal arrangement as proven by X-Ray Scattering when the synthesis is carried out with MCM-41, which shares the same arrangment of pore with SBA-15, but inherently doesn't exhibit microporsity connecting the individual mesopores. [3] This means, that after attempted synthesis of CMK-3 using MCM-41 as a template, only disordered, singular nanowires are obtained, which obviously cannot be arranged in a hexagonaly ordered 2-D lattice. Jain et al. [17] also showed in their work, that these interconnections are probably also vital to the overall behaviour in ad- and desorption.

Because of the open nature of the pore space between the strictly ordered carbon nanowires, no clear pore size can be assigned. Still, a pronounced capillary condensation event can be observed in sorption measurements of CMK-3, which led Jun et al [4] to assign the largest inscribed radius between three adjacent rods to be the pore space (figure 1). A rough estimation of the dominant pore size from X-Ray and sorption data seem to prove this simplified model. Gor et al [16] extended on this description of the open void space and fitted a QSDFT kernel of cylindrical pores to the adsorption and desorption branch, resulting in a pore size distribution which also had its maximum close to

largest inscribed radius.

B. Experimental Methods

a. Characterisation from Scattering The CMK-3 material in this work was characterized in-house at the Montanuniversitt Leoben with a Bruker Nanostar unit with a $Cu - K_\alpha$ Iμs X-ray micronsource with a wavelength of λ being $0.154nm$, two 300 μm SCATEX pinholes for collimation and the measurement distance set at 65 cm. The sample powder was situated in a custom sample holder and fixed between two Scotch tapes. The exact distance between the sample and the detector (VANTEC 2000) was determined with AgBh, which was also mounted on the same sample holder. Transmission was determined by Glassy Carbon measurements with and without the sample after each measurement of the CMK-3. The background from the tape was consequently corrected for transmission and then subtracted from the measured pattern to obtain correct Small Angle X-Ray Scattering (SAXS) patterns, which were then reduced to 1-D curves in q-space in nm^{-1} by custom in-house software. The overall definition of q and its relation to the scattering angle 2Θ is given by:

$$q = \frac{4\pi}{\lambda} sin(\Theta) \tag{1}$$

with λ being the wavelength of the scattered X-Rays.

b. Evaluation of Scattering Data Small Angle X-Ray Scattering is an indirect experimental method which essentially probes the electron density difference between all phases present in a sample [20]. Because of its indirect nature, systems containing multiple scattering phases or materials with very complex geometries are very hard to evaluate. This is why one usually tries to simplify the measurement by either reducing the amount of phases present in a sample and choose materials with a known structure. The great advantage of materials such as CMK-3 is that the geometry is very well known [4] [3] and that the amount of scattering phases is limited to the Carbon alone in an evacuated sample. In CMK-3, the scatterers which are of note in the measurement are the nanowires themselves, which are usually represented by infinitely long cylinders with a radius r_0. For a hexagonal, 2-dimensional system of individual scatterers the peak position is uniquely defined by:

$$q_{hk} = \frac{4\pi}{3^{\frac{1}{2}} D} (h^2 + k^2 + hk)^{\frac{1}{2}} \tag{2}$$

with q_{hk} being the value at which the peak with the Miller indices h and k for a nanowire distance of D is measured. If h and k are equal or one of them is zero, the multiplicity M of the structure factor for this Bragg peak is 6, if h and k are not equal the multiplicity is 12. This allows the exact measurement of the nanowire separation from experiment. But Small Angle Scattering can also provide additional information on the overall porosity via the scattering invariant [20] and by model fitting. For any two phase sample, in this case describing the carbon and empty space in the material, one can easily determine the volume fractions of both phases from the scattering invariant, which reads as:

$$Q = \int_0^{\inf} I(q) q^2 dq = 2\pi\rho^2\phi(1-\phi) \tag{3}$$

with $I(q)$ being the recorded intensity at the angle q, ρ being the difference in electron density between both phases in the system and ϕ being the volume fraction of one of the phases. If we know the electron density difference between both phases in the sample, we can consequently calculate the volume fractions. If the skelettal density of the Carbon material would be known in our case, we could calculate the electron density of the material because we can very simply determine the amount of electrons per Carbon atom. Because we unfortunately don't know the actual skelettal density of our Carbon material, we cannot infer the phase fractions of the void and solid phases, so we need to resort to modelling. The probably most suitable technique was first introduced for SBA-15 by Zickler et al in 2006 [21]. In the case of SBA-15 one can assume a completely hollow core centered in the cylindrical pore, a hollow cylinder with a certain thickness around the hollow core which represents the so called corona [21] and another infinitely thick, hollow cylinder which doesn't contribute to the scattering because of its size. Every single of these cylinders is then identified by its specific electron density, determining the overall scattering intensity. The corona in the model represents a transition zone in the pore in which surface corrigations and surface roughness are blurred to achieve a electron density somewhere between the solid material and the void. We will omit the existence of pronounced surface roughness and simplify the model, meaning we describe the carbon nanowires as perfectly smooth, infinitely

long cylinders. Because CMK-3 is basically the inverse of SBA-15 [22] and Small Angle Scattering is only sensitive to differences in scattering length density, which in this case is proportional to the electron density of the material, we should be able to apply the reduced model

$$I(q) = kS(q)F(q)^2 \tag{4}$$

with k being a constant factor, $S(q)$ the structure factor defining the angle at which Bragg peaks are observed and $F(q)$ being the form factor of a infinitely long cylinder

$$F(q) = \frac{2J_1(qr_0)}{qr_0} \tag{5}$$

with r_0 being the rod radius and J_1 being the Bessel function of the first kind and first order. The singular Bragg peak should then exhibit the integrated intensity $I_{hk}(q)$, which is then only dependent on the form factor $F(q)$ squared. Hence, for every recorded peak, the following equation [21] must hold:

$$\frac{I_{hk}}{M} = kF(q)^2 \tag{6}$$

which means that the from factor uniquely determines the measures intensity at the respective q-vales. Then the difference between the integrated intensities of the individual peaks and the form factor have to be minimized, which results in a distinct value for the rod radius r_0[21]. Because we then have definitively identified the nanowire spacing D and the Carbon rod radius r_0, we can then calculate the geometrical features of the CMK-3 material. The largest inscribed radius as indicated by the blue circle in figure 1, which is used as the actual pore size in Gor et al. [16], is then given by:

$$r_u = \frac{D}{3^{\frac{1}{2}}} - r_0 \tag{7}$$

and the smallest inscribed radius in the void space indicated by the green circle in figure 1 is then calculated by:

$$r_i = D - 2r_0 \tag{8}$$

c. Characterisation from Sorption The Nitrogen adsorption isotherm was recorded by our partners from the Paris-Lodron University, Salzburg, on a Quantachrom instrument at 77.4 K.

C. Theoretical Methods

In this section we introduce several key concepts in the theoretical description of sorption in CMK-3 :

- Variational Methods in Sorption
- Equivalence of Variational and Thermodynamic Descriptions
- General inverse-power-law Potential for Cylindrical Rods: The Cole-Saam Approach

All the derivations in this part are based on the fact that the aspect ratio between the diameter of the rods in our system and their length is close to zero, meaning that we can describe sorption purely in a plane perpendicular to the rods. Because of the radial symmetry of the carbon rods themselves and the hexagonal arrangement of the carbon rods, it is advantageous to use cylindrical coordinates in the derivations in this section.

1. Variational Methods in Sorption

The calculus of variations [23] is the basis of analytical mechanics and is mainly concerned with the minimization of so called functionals. In contrast to typical extremal calculations which are only concerned with the minimization or maximization of functions, functionals are basically "functions of functions". Typically one seeks to extremise functionals in the form of

$$L = \int_b^a f(t, q, q')dt \tag{9}$$

with the actual shape of the function not known. Sorption phenomena are usually modelled in the framework of the Grand Free Energy Ω, which can be treated as a functional to be minimized. To obtain a usable description of the Grand Free Energy, we employ cylindrical coordinates as stated above. Hence, from now on we use equation 9 in the form:

$$\Omega = \int_{\theta_0}^{\theta_1} f(\theta, l, l_\theta) d\theta \tag{10}$$

with θ_0 and θ_1 being the limits of the angular interval we inspect, l being the distance from the origin as a function of θ at which the interface between vapor and liquid is situated and l_θ being the the derivative of l with respect to θ. For adsorption in CMK-3 type materials there are three fluid phases we need to consider, which we will describe as

- separated: there is only a thin film present on every singular rod
- bridged: the rods are connected via thin liquid bridges
- filled: the whole pore space is filled with liquid

Every single one of these phases should be characterized by a pronounced minimum in the Grand Free Energy and hence exist in a real world CMK-3 material.
To describe the bridged case, it is easier to set the origin of the cylindrical coordinate system in the middle of the void spaces interstitial[8] (see figure 3). Consequently, the Grand Free Energy can be expressed for CMK-3 type materials as [8]

$$\begin{aligned}\Omega(l(\theta)) = 6 \int_0^{\pi/3} d\theta(\gamma(l^2 + {l_\theta}^2)^{1/2}) + \\ +\Delta\mu[R^2 3^{\frac{1}{2}} - \frac{\pi}{2} r_0^2 - 6 \int_0^{\pi/3} d\theta \frac{1}{2} l(\theta)^2] + \\ +6 \int_0^{\pi/3} d\theta V(l, \theta)\end{aligned} \tag{11}$$

with R and r_0 as defined from figure 1. The first part of the equation describes the contribution of the interfacial energy γ, the second term describes the influence of the chemical potential μ of the adsorbed liquid and the last term describes the energy due to the film potential. The last contribution can be calculated via the volume of the gas phase in the open pore space, which connects film potential, like the popular Disjoining Pressure Π [24], to the function V

$$V(l, \theta) = \int_{l(\theta)}^{l_{max}} \Pi(l, \theta) l dl \tag{12}$$

l_{max} is the maximal value of the profile to be considered, which helps keeping the integration limited to a unit cell in ordered systems. The geometrical relations describing the case of the bridged solution are depicted in figure 3. The integration takes place in the unit cell highlighted by the green triangle, while the vector describing the film, l_Θ is also shown. The film potential Π we chose for our study was the Frenkel-Halsey-Hill equation [25], but the simplification that the film potential is only due to a single rod is not applicable here and leads to an overestimated film growth in the simulations. Hence we adopted the approach from Ref [8] and summed the potential of all three rods in the unit cell at each single point of consideration. Applying the Euler-Lagrange equation to Eq.11 leads to the differential equation, which minimizes the free energy in any radially symmetric case, which reduces to Derjaguins equation for cylindrical pores [5]. Multiplying both sides of Eq. 11 with $\frac{r_0}{\gamma}$ gives us a unitless representation, but because this will be easier seen when the functional has been already minimized, we will introduce the unitless representation later.
The Grand Free Energy can be also calculated for the separated and completely filled phase. If we consider the separated phase, describing film formation on the individual cylinders, we set the origin of our coordinate system in the center of the rod [8][14][26] and Eq 11 becomes [8]:

$$\begin{aligned}\Omega(l(\theta)) = 6 \int_0^{\pi/6} d\theta(\gamma(l^2 + {l_\theta}^2)^{1/2}) + \\ +\Delta\mu[6 \int_0^{\pi/6} d\theta \frac{1}{2} l(\theta)^2 - \frac{\pi}{2} r_0^2] + \\ +6 \int_0^{\pi/6} d\theta V(l, \theta)\end{aligned} \tag{13}$$

The geometrical relations are depicted in figure 4. Because we still use symmetry to ease the computational load and the inscribed angle in every edge of the triangle is $\frac{\pi}{3}$, the upper bound of the integral is reduced to $\frac{\pi}{6}$. This is only due to the change of the origin of the polar coordinate system from the center of the void space to the center of the rod.
In the case of the completely filled pore space the Grand Free Energys sole contribution is the liquid inside the filled pore

$$\Omega(l(\theta)) = \Delta\mu[R^2 3^{-\frac{1}{2}} - \frac{\pi}{2}r_0^2] \tag{14}$$

Because we don't expect any radially non-varying profiles, the whole profile can now be minimized by means of Variational Calculus. This means, that we have to apply the Euler-Lagrange equation to equations 11 and 13, with the Euler-Lagrange equation being:

$$\frac{d}{d\theta}\frac{\delta\Omega(l, l_\theta, \theta)}{\delta l_\theta} = \frac{\delta\Omega(l, l_\theta, \theta)}{\delta l} \tag{15}$$

To apply equation 15, we rewrite equations 11 and 13 to get a clearer picture:

$$\begin{aligned}\Omega(l(\theta)) = 6\int_0^{\pi/6} d\theta(\gamma(l^2 + l_\theta^2)^{\frac{1}{2}} + \\ +\Delta\mu\frac{1}{2}l(\theta)^2 + V(l,\theta)) + \Delta\mu r_0^2\frac{\pi}{2}\end{aligned} \tag{16}$$

$$\begin{aligned}\Omega(l(\theta)) = 6\int_0^{\pi/3} d\theta(\gamma(l^2 + l_\theta^2)^{\frac{1}{2}} - \\ -\Delta\mu\frac{1}{2}l(\theta)^2 + V(l,\theta)) + \Delta\mu(R^2 3^{\frac{1}{2}} - r_0^2\frac{\pi}{2})\end{aligned} \tag{17}$$

where equation 16 represents the separated case and equation 17 the bridged case. The actual functional to be minimized is per definition of functionals the integration term and can be treated like a classical differentiation operation. The variation with respect to q' or actually l_θ is the same for both equations and reads as:

$$\frac{\delta\Omega}{\delta l_\theta} = \frac{l_\theta}{(l^2 + l_\theta^2)^{\frac{1}{2}}} \tag{18}$$

Because of the difference of the origin between the bridged and separated case, we once have the contributing term of the liquid phase to be positive in the separated case and negative in the bridged case. Hence we get for the right part of equation 15

$$\frac{\delta\Omega(l(\theta))}{\delta l} = \mp(\Delta\mu l - \Pi(l,\theta)l) + \gamma\frac{l}{(l^2 + l_\theta^2)^{\frac{1}{2}}} \tag{19}$$

Hence we can simply apply the Euler-Lagrange equation to our problem if we plug in equations 18 and 19 into equation 15. The differential equation resulting[8]is of second order, non-homogeneous and represents a two point boundary value problem:

$$\begin{aligned}0 = \gamma\frac{d}{d\theta}(\frac{l_\theta}{(l^2 + l_\theta^2)^{\frac{1}{2}}}) - \\ -\gamma\frac{l}{(l^2 + l_\theta^2)^{\frac{1}{2}}} \\ \pm l(\Delta\mu - \Pi(\theta, l))\end{aligned} \tag{20}$$

The positive sign corresponds to the seperated case, whereas the negative sign gives bridged solutions.[8] To solve equation 20, we applied a finite differences approach, which requires two Dirichlet, two Neumann or mixed boundary conditions. In our case, we only have definite Neumann boundary conditions, meaning we have values for the differential of l with respect to θ at the boundaries. The boundary conditions are in the bridged case as depicted in figure 3, with the origin fixed at the center of the interstitial void space:

$$l_\theta = 0 \quad at \quad \theta = 0 \quad and \quad \theta = \pi/3 \tag{21}$$

For the separated case, where the origin is set on the center of a single rod as shown in figure 4, the conditions read as:

$$l_\theta = 0 \quad at \quad \theta = 0 \quad and \quad \theta = \pi/6 \tag{22}$$

The Grand Free Energy of the solutions to equation 20 corresponding to the bridged and separated phase respectively, need to be compared to see which phase exists at a given relative pressure. These also have to be compared to equation 14 to conclude which phase exists. To simplify the numerical solution finding and parameter studies, we resort to using the unitless version:

$$\begin{aligned} 0 = \frac{d}{d\theta}\left(\frac{l_\theta}{(l^2 + l_\theta^2)^{\frac{1}{2}}}\right) - \\ - \frac{l}{(l^2 + l_\theta^2)^{\frac{1}{2}}} \\ \pm l(\Delta\mu' - \Pi(\theta, l)') \end{aligned} \tag{23}$$

with $\Delta\mu'$ and Π' being the unitless energies corresponding to:

$$\Delta\mu' = \frac{\Delta\mu r_0}{\gamma} \tag{24}$$

$$\Pi' = \frac{R_g T k r_0}{v_l \gamma}\left(\frac{h_0}{r_0^{\frac{1}{m}}}\right)^m \tag{25}$$

The last equation only has this form, if we use the Frenkel-Hasley-Hill isotherm [25], which is a popular choice in the field of sorption.

$$\Pi(h) = -\frac{kTR_g}{\left(\frac{h}{h_0}\right)^m} \tag{26}$$

with k,h_0 and m being the fitting parameters. The large popularity is due to the fact that it represents a more general approach to interaction forces between molecules, which are usually taken to be of the power -6 in the case of Van-der-Waals dispersion forces. In this work we will also apply a suitable film potential for cylinders, be the overall unitless representation is not affected by this choice. The 2-point boundary value problem is then finally formulated as:

$$l_{\theta\theta} = 2\frac{l_\theta^2}{l} + l \pm \frac{(l^2 + l_\theta^2)^{\frac{3}{2}}}{l}(\Delta\mu' - \Pi') \tag{27}$$

Equation 27 is equivalent to the DBdB equation of sorption, if we assume cylindrical symmetry. Hence, in this case l doesn't vary with θ and the derivative l_θ is therefore zero. Also,Π is not dependant on θ anymore. Plugging this into equation 27, we get:

$$\begin{aligned} l_\theta &= 0 \\ 0 = \gamma\frac{d}{d\theta}\left(\frac{0}{l}\right) - \gamma\frac{l}{(l^2 + 0^2)^{\frac{1}{2}}} &\pm l(\Delta\mu - \Pi(l)) \\ 0 &= -\gamma \pm l(\Delta\mu - \Pi(l)) \\ \gamma/l + \Pi(l) &= \pm\Delta\mu \end{aligned} \tag{28}$$

In the cylindrical case l is equal to the pore radius R_{zyl} minus the film thickness h. For layering, we have to take $\Delta\mu$ to be positive, which is with the definition of the parameter:

$$\Delta\mu = -R_g T log(\frac{p}{p_0})/v_l \tag{29}$$

put into equation 28 resulting in:

$$R_g T log(\frac{p}{p_0}) = -v_l(\frac{\gamma}{(R_{zyl} - h)} + \Pi(h)) \tag{30}$$

with R_{zyl} being the radius of the cylindrical pore and h representing the film thickness. This equation is exactly the same as in the DBdB Theory [5] for cylindrical pores. Hence, this is a hard test for the assumptions described above

and proves the applicability of this approach. Also, this allows us to describe the sorption process on the outside of a singular cylinder, which is the case in our CMK-3 type system. In this case only the argument in Π and the denominator for γ changes.

$$R_g T log(\frac{p}{p_0}) = -v_l(\frac{\gamma}{(r_0+h)} + \Pi(r_0+h)) \tag{31}$$

with r_0 being the radius of the cylinder where sorption takes place on.
This equation shows the applicability of the variational approach to describing sorption in these systems. But equation 27 can then also be used to describe the general equation for sorption in the DBdB frame work if we reshape it to:

$$\begin{aligned} l_{\theta\theta} &= 2\frac{l_\theta^2}{l} + l \pm \frac{(l^2+l_\theta^2)^{\frac{3}{2}}}{l}(\Delta\mu' - \Pi') \\ 0 &= -l_{\theta\theta}l + 2l_\theta^2 + l^2 \pm (l^2+l_\theta^2)^{\frac{3}{2}}(\Delta\mu' - \Pi') \\ 0 &= \frac{-l_{\theta\theta}l + 2l_\theta^2 + l^2}{(l^2+l_\theta^2)^{\frac{3}{2}}} \pm (\Delta\mu' - \Pi') \end{aligned} \tag{32}$$

The first term of equation 32 is equivalent to the general curvature κ in cylindrical coordinates, hence this reads as:

$$\begin{aligned} \kappa &= \frac{-l_{\theta\theta}l + 2l_\theta^2 + l^2}{(l^2+l_\theta^2)^{\frac{3}{2}}} \\ 0 &= \kappa \pm (\Delta\mu' - \Pi') \\ now \quad &reforming \quad to \quad units \\ 0 &= \kappa\gamma \pm (\Delta\mu - \Pi) \end{aligned} \tag{33}$$

which is exactly the same equation as presented in Ref [5]. This means that the approach discussed so far is a generalization of other traditional descriptions like Brokhoff and De-Boer developed in their earlier, seminal works [5].

2. Equivalence of Variational and Thermodynamic Descriptions

We will introduce the equation in the spirit of Brokhoff and De-Boer [5], but will keep the notation as introduced earlier in this work. We start by expressing the differential of the Free Gibbs Energy G as

$$\mathrm{dG}_{p,T} = \gamma \mathrm{dA} + \mathrm{dN}(\Pi - \Delta\mu) \tag{34}$$

where γ is the surface energy of the liquid vapour interface, and $\Delta\mu$ is the potential of the vapour and Π the potential of the adsorbed layer. To get the actual expression, the change of the chemical potential G cannot change with the amount dN in the system, leading to

$$\frac{\mathrm{dG}}{\mathrm{dN}}_{p,T} = \gamma\frac{\mathrm{dA}}{\mathrm{dN}} + \Pi - \Delta\mu \tag{35}$$

where $\frac{\mathrm{dA}}{\mathrm{dN}}$ is expressed as

$$\frac{\mathrm{dA}}{\mathrm{dN}} = -\left(\frac{1}{R_2} + \frac{1}{R_1}\right) v_l \tag{36}$$

with R_1 and R_2 are the principal radii of curvature. From now on we will express the curvature as κ and introduce it in Eq.35 and equate Eq.34 to zero

$$\frac{\mathrm{dG}}{\mathrm{dN}}_{p,T} = \gamma\kappa v_l + \Pi - \Delta\mu = 0 \tag{37}$$

which ends up, after rearrangement to

$$\Delta\mu = \Pi + \gamma\kappa v_l \tag{38}$$

The general meaning of the equation is that by minimizing the Gibbs Free Energy, we have found a description of the equilibrium configuration of our system at a given pressure. This is true for any kind of geometric shape of the

pore space but not exclusive to a certain phase. By introducing curvature κ as a differential and determining the initial or boundary conditions describing the geometry satisfactorily, we arrive at an expression which describes a stable liquid vapour profile. This is true for any kind of configuration, below or at and above the pressure of capillary condensation. This means that equation 27 as developed in this and in the preceding part is suited to accurately describe the film profile of the separated and filled solution. Although we can accurately describe the competing phases, this is technically not a totally sufficient criterion for phase transition for any condensation event. In contrast to equation 27, v_l is not yet integrated in the chemical potential $\Delta\mu$.

3. General power-law Potential for Cylindrical Rods: The Cole-Saam approach

To calculate the dependence of the chemical potential on the film thickness for our system, we tried for a more physical approach than the more popular disjoining pressure in the Derjaguin Borkhoff de Boer approach [11]. Cole and Saam [27] published a theory in the seventies, which makes use of the Van-der-Waals interaction between the substrate wall and the fluid molecules to describe the dependence of the chemical potential on the film thickness. These and later works have mainly been focused on cylindrical pores [27][28], for which the interaction potential of the adsorbing species with the substrate was governed by an interaction factor and another, multiplicative argument based on the geometry of the pore. In our material, and hence in all CMK-3 like materials, the situation is quite different because of the convex nature of the mesopores. Consequently, a different potential function has to be applied for these kinds of material. J.R. Philip [29] derived appropriate potentials in the late seventies, where he calculated the interaction for arbitrary inverse-power-law potentials for several substrate geometries including singular rods. To achieve his result, let us consider a single point outside a singular rod at a distance d from the center from the rod. Hence, we want to compute the interaction energy of the rod with the singular point, which is easiest when we calculate all the interaction energies for all the points on a cylindrical shell at a distance l_0^* from the center of the rod and move outwards from its center to its surface, always assuming power-law forces between each shell and the point at which we want to calculate the integral at. Because of the centrosymmetricity of the rod, we only need to consider a singular line passing through its center. The solution of the integral was calculated by Philip [29] and will be applied in this work.

$$\Pi(h) = \frac{\pi^{3/2}\Gamma\left(\frac{\epsilon-1}{2}\right)}{\Gamma\left(\frac{\epsilon}{2}\right)} \alpha r_0^2 \left(r + r_0\right)^{1-\epsilon} {}_2F_1\left(\frac{\epsilon-1}{2}, \frac{\epsilon-1}{2}; 2; \left(\frac{r_0}{h+r_0}\right)^2\right) \tag{39}$$

where Π is the film potential, α is the interaction parameter and ϵ is the power of the inverse-power-law. The parameters α and ϵ which are determining the interaction for the function are fitted from reference isotherms, assuming infinite, planar substrates in any case. This reduces equation 39 to:

$$\Pi(h) = -\frac{(2\pi\alpha)h^{3-\epsilon}}{(\epsilon-3)(\epsilon-2)} \tag{40}$$

which is very similar to the Frenkel-Halsey-Hill depiction of the film potential and consequently the same as the Disjoining pressure as applied in other works[11]. It can actually be directly related to the parameters of the Frenkel-Halsey-Hill isotherms with:

$$m = 3 - \epsilon \tag{41}$$

$$R_g T k h_0^m = \frac{2\pi\alpha}{(\epsilon-3)(\epsilon-2)} \tag{42}$$

These parameters are used to more accurately describe the potential of a singular Carbon nano-wire. As mentioned above, we also consider the potential of all the rods in the CMK-3 unit cell by summing over the shortest distances between the singular rods and the point we want the potential to be calculated at.
The actual interaction parameters used in this study for nitrogen were obtained from a reference isotherm from literature [30]. The significance of the Cole-Saam approach is also represented in the fact, that the structure of the solid is represented in the potential. In cylindrical pores, this leads to a small difference between the flat solid approximation [29]. The reason for this lies in the calculation of the potential, which basically breaks down to the integration of the interaction of a solid volume dV and an arbitrary point close to the surface. In the case of a cylindrical pore, there is a lot of material present at all directions which needs to be considered, hence resolving in a result relatively close to a flat surface. In the case of a cylindrical rod this is not the case, meaning that the overall potential is reduced when compared to the flat and cylindrical case.

III. RESULTS

1. Experimental Results: Adsorption and Scattering Measurement Characterization

a. Characterisation from Sorption Measurements: For the CMK-3 material our partners measured nitrogen ad- and desorption, a double step transition is barely visible. The first transition at 0.5 $\frac{p}{p_0}$ is dominant and second, slight step-like transition is visible at 0.7 $\frac{p}{p_0}$ in figure 2b. The desorption branch in the aforementioned figure exhibits only one distinguishable evaporation event. This is very much in line with other measurements which can be found in [4] [16] [15] etc. The pore size distribution derived from NLDFT exhibits two sharp maxima at 3.25 and 4 nm, which is significantly lower that the result obtained from Gor et al in 2012 [16]. Also, the pore size distribution shows non zero fractions at larger pore sizes, which is related to the ascending nature of the sorption isotherm. This shouldn't heavily affect the result for the main adsorption events which are signified by the two maxima and could be related to the packing of the CMK-3 powder.

b. Characterisation from Scattering Measurements Another interesting point about the determination of pore size has to be made in relation to the Small Angle X-Ray Scattering data. From the scattering curve on the CMK-3 powder in our work we can easily distinguish the rod-spacing by calculating the center of mass of the peak. The resulting value for the lattice parameter from the SAXS pattern shown in figure 2a is close to 10.05 nm. We can also clearly observe not only the dominant (10) peak, but also two higher order peaks with the Miller indices (11) and (20). Unfortunately we can only distinguish these three distinct peaks, which decreases the overall significance of the result obtained from the fit. Contrary to the proposed pore diameter of around 4.7 nm by Gor et al. [16], meaning the largest inscribed radius (see figure 1) between 3 adjacent rods [4], we arrive at a pore size of 3.35 nm, with the smallest surface to surface distance between two adjacent rods being 1.8 nm. The discrepancy between both kinds of measurement are large in relation to the mean structure size in the system. This could be either related to the simplification we introduced in the evaluation of the scattering pattern by describing the nanowires as smooth cylindrical rods or a gross error in the estimation from adsorption measurements.

2. Theoretical Profiles and Phase Diagrams

A theoretical phase diagram was calculated for systems for the set of interaction parameters, which are presented in table I. In this phase diagram the existing phases in our system, meaning separated, bridged and filled, is depicted as a function of the fraction of the nanowire distance to nanowire diameter and the relative pressure $\frac{p}{p_0}$. The existance of each phase was determined by selecting the lowest Grand Free Energy at each relative pressure. The interaction parameters were obtained from published reference isotherms of Nitrogen on Carbon Black and fit with a FHH isotherm. Because it can be assumed that the curvature of the Carbon substrate was substantially smaller and therefore not in the range of the thickness of the layers, we can use these parameters and equate them to equations 41 and 42. This allows us to use the more exact formula 39 from here on. Because equation 27 is a non-linear ordinary differential equation of second order with Neumann boundary conditions, no standardized solution method exists. Also, no sufficient description of the solution process was given in Ref [8], but a cryptic reference to a relaxation method. To clarify and further the application of the variational description in physisorption, we give a more detailed analysis of the solution process.
The simulations were conducted with a self written Python module using the integrated development environment *Anaconda*. To solve this specific problem, we chose to discretize the differential equation on a set of equidistant mesh points and define a residual, which is the second vector norm of the discretized differential equation. Consequently, a profile that minimizes the residual should yield the requested solution, which means we have reduced the solution of the differential equation to a root finding problem. Still, equation 27 represents a stiff differential equation, meaning that initial solutions which are too far off the final solution won't give a converged result. Hence, it is necessary to further specify the criteria which guarantee convergence to a unique solution in the bridged case. To attain consistent convergence, one has to critically contemplate the method and the methods parameters employed by different algorithms to find the root of a vector function. Most algorithms utilize the Jacobian matrix to calculate gradients of the input function and then calculate the intermediate solution given a certain step size. Because the potential land scape of equation 11 yields several minima corresponding to the completely filled, the separated and bridged phase, small step sizes can result in slow convergence rates or convergence on a solution which actually don't minimize the Grand Free Energy. To achieve convergence for the bridged case, a larger stepsize of 10^{-2} was necessary for the evaluation of the Jacobian, which lead to consistent bridged solutions with a smooth liquid vapour interface

profile. Conversely, it is not hard to find consistent solutions for the separated case.
A second important point is the selection of a initial solution, from which we obtain the final, converged solution. It is of advantage, that the supplied profile which we supply as the initial guess also satisfies the boundary conditions 21 and 22 for the differential equation 27. For the separated case, it is sufficient to supply a constant profile which automatically satisfies the boundary conditions to achieve consistent convergence. Closer inspection of the profile obtained gave slight variations of the film thickness on the nanowire, but the difference in dimension was so small that further discussion is not necessary in the scope of this work. In the bridged case this is not achieved by a constant profile, hence we choose a cosine function with appropriate upper and lower bounds. For the hexagonal arrangement of carbon rods we also have to take into account, that a simple cosine profile could intersect the carbon rod in our simulation. The work around we applied is to seed the values of the argument of the cosine according to a simple powerlaw function, which distorts the function accordingly if we apply the result to the original mesh points. This gives us an initial solution which not only satisfies the boundary conditions and doesn't violate the geometrical bounds of our system, but also consistently converges to a smooth solution to equation 27. The overall solution process for 30 relative pressures per considered $\frac{D}{r_0}$ value came out to be around two minute on a modern laptop. Upon solving the differential equation 27, we applied it to a hexagonal and a squared arrangement of carbon nanowires, corresponding to a CMK-3 type material and the arrangement as depicted in the paper from Dobbs [8]. To get information on the influence of the geometrical arrangement and because we can assume that the interaction parameters for Nitrogen are basically universal [5], we systematically vary the diameter of the carbon nanowires with a set spacing. Also, we have to assume that the distance between rod centres, which we can easily get from Small Angle X-Ray Scattering, shouldn't vary significantly in a macroscopic sample. Also, because Small Angle Scattering probes relatively large sample volumes, the spacing of the nanowires is a statistically significant mean. Varying the nanowire diameter and not the rod spacing is in contrast to the work by Yelpo [18], in which not the diameter of the nanowires was varied, but the distance between them. Because it is computationally expensive and probably time consuming to recalculate the Lennard Jones potential for every single rod diameter considered, this approach makes sense, but it completely dismisses the effect of the substrate curvature on the adsorption process. Also, if the distance of the carbon nanowires would vary significantly enough to generate a pore size distribution comparable to the one retrieved in the paper of Yelpo [18] with a rod diameter of 3.5 nm and the mean poresize around 4.5 nm, the mean distance between the nanowires would be 13.5 nm. This value is significantly above the recorded lattice parameters we have encountered in experiment and literature for CMK-3 and gives us confidence in the approach we have chosen to vary the pore sizes. Consequently, the rod radius r_0 was varied between 3.3 nm and 4.4 nm in 0.05 nm steps, for a set rod distance $D = 2R$ of 10.1 nm. The rod distance and radius were calculated from the experiments and are in good agreement with the dimensions described in Refs. [4],[15] and [16]. Then, for the given set of interaction parameters, the profiles for the separated and filled case were calculated for 30 distinct, equally spaced relative pressure values ranging from 0.01 to 0.95, which coincides with the experimental solution in usual sorption experiments. The evolution of the profiles with increasing relative pressure coincides nicely and represents the expected result. In figure 4, several profiles for the bridged case in the hexagonally arranged system are shown. As can be clearly distinguished, the overall size of the void space at the center of three neighbouring rods decreases with growing relative pressure. Once the profile has reached near circular form, the filled phase gets more favourable and condensation takes place. From these profiles, we calculate the Grand Free Energies corresponding to each phase and pressure and plotted them against each other. With 30 different pressure values, we can expect the overall shape of the curves of the Grand Free Energies to be sampled satisfactorily. A sample diagram of the evolutions of the Grand Free Energies is shown in figure 7. The present phase is determined by it exhibiting the lowest Grand Free Energy compared to the other possible phases. Via interpolation and root finding, we can consequently get the exact relative pressure values at which a phase transition should occur in desorption. Of note is also the discontinuity which is visible for the separated case in figure 7. Upon further inspection, the relative pressure of the dicontinuity coincides with a profile at which the local thicknesses of neighbouring rods have reached values at which the profiles would overlap, meaning the void space indicated by the green disk in figure 1 would be completely filled. This discontinuity in the solutions found for the separate case appears at lower relative pressures with increasing nanowire diameter relative to the rod spacing.
From the information on the Grand Free Energies we can extract phase diagrams on the desorption as a function of relative pressure and the ration of $\frac{D}{r_0}$. This fraction can be related to the maximum inscribed radius r_u* which reads for the hexagonally arranged system as presented in 7 which can always be expressed without units:

$$r'_u = \frac{r_u*}{r_0} = \frac{D}{r_0}\frac{1}{3^{\frac{1}{2}}} - 1 \tag{43}$$

linking the reduced sizes to the pore geometry considered in earlier works [4]. A very similar relation holds for the quadratic arrangement:

$$r_u* = \frac{D}{2^{\frac{1}{2}}} - r_0 \tag{44}$$

TABLE I. Parameters of the FHH-Isotherm

Adsorbate	k	m
Nitrogen	61.7	2.51

which can again be rearranged to a unitless form:

$$r'_u = \frac{r_u*}{r_0} = \frac{D}{r_0}\frac{1}{2^{\frac{1}{2}}} - 1 \tag{45}$$

In figure 8 we show the resulting phase diagrams for the interaction parameters from table I. The difference between phase diagrams for the hexagonally and quadratically arranged Carbon rods is clearly visible. Because we used the same rod radii and rod distances in both simulations, the influence of the surface tension on the separate solutions should be negligible, which means that the differences can only be due to the geometric arrangement of the rods.
Still, for every phase diagram calculated the same overall trend can be observed. With increasing pore space, the bridged phase gets less favourable and occurs at higher relative pressures, while it is immediately present in the case of narrow voids. Interestingly enough, the capillary condensation describing the transition from the bridged phase to the completely filled phase is not that strongly dependant on the geometrical arrangement and over size of the structures in the material.

IV. DISCUSSION

The fundamental problem in sorption measurements for more complex geometries like in CMK-3 is that it cannot be described unambiguously by a single parameter. Cylindrical pores are easily described by a singular parameter, meaning the pore radius assuming that they are practically infinitely long. For CMK-3, we need at least two separate parameters to clearly define the pore space. The concept of one singular radius inscribed in the void space between three adjacent rods is actually not very indicative by itself, because a numerical value can be realised by a multitude values for the rod spacing D and the rod radius r_0 when plugged into equation 7. In the case of characterization of materials via ad- and desorption one usually assumes interaction parameters for the adsorbate and substrate and fits the pore size distribution accordingly. With a singular measurement, we can consequently only determine one parameter and not multiple ones, which in turn means that to unambiguously identify the geometry of a porous, convex material additional measurements are needed. In our case we resort to small angle scattering to attain more knowledge. The analysis of the peaks gave us a minimal distance between rods of 1.8 nm and a largest inscribed radius in between three adjacent Carbon rods of 3.35 nm for a nanowire distance D of 9.95 nm. The single rod radius comes out at 4.05 nm, which gives us a $\frac{D}{r_0}$ ratio of roughly 2.45. If we compare this with the phase diagram in figure 8, we can clearly see that the predicted condensation events clearly don't match with the values for the sorption isotherm in figure 2,b. If we analyse the phase diagrams depicted in figure 8, several features are obvious. For both phase diagrams, we can observe that with increasing ratio of the lattice spacing $D = 2R$ over the rod radius r_0, the interval of existence for the bridged phase is narrowing. As stated in Ref. [8], this is a result of the increasing contribution of the surface tension, because the surface area of the vapour liquid interface increases with increasing D to r_0 ratio. It also follows the general intuition that with decreasing pore size, here meaning a decreasing $\frac{D}{r_0}$ ratio, the capillary condensation and evaporation occurs at lower relative pressures. The general shape of the phase diagram for the quadratic arrangement of the carbon nanowires aligns quite nicely with the shape shown in Dobbs original paper [8] for the transition from the separated to the bridged phase. But in contrast to the previously cited work, the transition from the bridged to the filled phase doesn't shift to higher relative pressures with decreasing pore size, but happens at lower relative pressures. Following the shape of the profiles we obtained for the bridged phase with increasing pressure, this seems the more physical solution to us.
Also, comparing both phase diagrams, we can distinguish the effect of the geometrical arrangement of the carbon nanowires relative to each other. The only difference between both cases is the potential of the system which we achieved by summing over every single contribution from every rod in the unit cell at each point considered. The potential Π at the intercept of the plane of symmetry and the distance between adjacent rods is higher in the case of the quadratic alignment, which seems to favour the separated phase over the bridged phase in this case.
The urgent question we need to answer now at last is if the results from Small Angle X-Ray Scattering and from the phase diagram for the hexagonally ordered Carbon nanowire system. To check, we simply compare the capillary condensation events at 0.5 and 0.7 $\frac{p}{p_0}$ in figure 8 and get a $\frac{D}{r_0}$ ratio of around 2.75. This translates with a rod distance of 10 nm to close to 3.6 nm nanowire radius and a largest inscribed circle radius of 4.3 nm. This closely aligns with the result from Gor et al [16] but is larger than the radius obtained from Small Angle X-Ray Scattering. The reason

for this discrepancy can likely be found in the overly simplified and crude model we used to retrieve the structural data from the measurement. It would probably be advantageous to include a corona into the model [21] to better describe the influence of the surface corrugations and surface roughness of the nanowires. The effective pore radius could then be estimated by also fitting the mean electron density of the corona and adjust the outer diameter of the nanowire accordingly to a phase fraction representing the amount of solid needed to achieve the fitted mean electron density of the corona.
Interestingly it seems as if the QSDFT method gives quite accurate results which could be due to the density gradient introduced in its wall. As we discussed earlier, it is still not entirely possible to then fully characterize the geometry of the CMK-3, because of the ambiguity of the definition of the mean pore size.

V. CONCLUSION

In this work we achieved the implementation of the variational approach into a Python module to calculate film profiles in periodic arrangements of cylinders. The program was then applied to Nitrogen sorption on hexagonal and quadratic arrangements of infinitely long carbon rods with different void fractions and the results converted into phase diagrams. The results indicate the existence of a bridged phase for the typical dimensions found in CMK-3 materials and therefore the existence of two capillary condensation events. Further, the results on the mean pore size were compared, with good agreement between our simulation and the value given by Gor et al [16], but a discrepancy between Small Angle X-Ray Scattering and the simulations. The reason for the difference in the results can be found in the overly simplified evaluation method applied to the scattering data, which means that future studies using a more refined approach will probably give good agreement between the methods. The program allows us to gain information on the existence interval of competing phases and also gives us the opportunity to calculate the distribution of liquid in porous media like CMK-3. The results from the program were compared to the results from Small Angle X-Ray Scattering and QSDFT [16] and show good agreement between the computational techniques and a significant discrepancy between the simulations and the measured values. Still, because of the ambiguity of the result from sorption alone, it should be good practice in the structure characterization to include techniques like Small Angle Scattering.
In the future, the results from this work will grant the possibility to derive kernels for characterisation and probably even give the opportunity to derive theoretical stresses in CMK-3 and alike materials.

ACKNOWLEDGMENTS

The author is thankful to the Marshall Plan Foundation for the funding of the research stay at the New Jersey Institute of Technology under the supervision of Dr. Gennady Gor, Dr. Gennady Gor and Dr. Oskar Paris for guidance and discussion, DI. Koczwara und Msc. Rumswinkel for the measurements of Small Angle X-Ray Scattering and Nitrogen sorption data on CMK-3.

[1] G. Y. Gor, P. Huber, and N. Bernstein, Applied Physics Reviews **4**, 011303 (2017).
[2] C. Balzer, A. M. Waag, S. Gehret, G. Reichenauer, F. Putz, N. Husing, O. Paris, N. Bernstein, G. Y. Gor, and A. V. Neimark, Langmuir **33**, 5592 (2017).
[3] R. Ryoo, S. Joo, S. Jun, T. Tsubakiyama, O. Terasaki, et al., Stud Surf Sci Catal **135**, 150 (2001).
[4] S. Jun, S. H. Joo, R. Ryoo, M. Kruk, M. Jaroniec, Z. Liu, T. Ohsuna, and O. Terasaki, Journal of the American Chemical Society **122**, 10712 (2000).
[5] J. Broekhoff and J. H. de Boer, Journal of Catalysis **10**, 368 (1968).
[6] P. I. Ravikovitch, G. L. Haller, and A. V. Neimark, Advances in colloid and interface science **76**, 203 (1998).
[7] P. I. Ravikovitch and A. V. Neimark, Langmuir **22**, 11171 (2006).
[8] H. Dobbs and J. Yeomans, Molecular Physics **80**, 877 (1993).
[9] G. Y. Gor, O. Paris, J. Prass, P. A. Russo, M. M. L. Ribeiro Carrott, and A. V. Neimark, Langmuir **29**, 8601 (2013).
[10] J. Prass, D. Müter, P. Fratzl, and O. Paris, Applied physics letters **95**, 083121 (2009).
[11] G. Y. Gor and A. V. Neimark, Langmuir **27**, 6926 (2011).
[12] J. Prass, D. Müter, M. Erko, and O. Paris, Journal of Applied Crystallography **45**, 798 (2012).
[13] C. Kresge, M. Leonowicz, W. J. Roth, J. Vartuli, and J. Beck, nature **359**, 710 (1992).
[14] J. Philip, The Journal of Chemical Physics **66**, 5069 (1977).
[15] K. Morishige and R. Nakahara, The Journal of Physical Chemistry C **112**, 11881 (2008).
[16] G. Y. Gor, M. Thommes, K. A. Cychosz, and A. V. Neimark, Carbon **50**, 1583 (2012).

[17] S. K. Jain, R. J.-M. Pellenq, K. E. Gubbins, and X. Peng, Langmuir **33**, 2109 (2017).
[18] V. Yelpo, V. Cornette, J. P. Toso, and R. H. López, Carbon **121**, 106 (2017).
[19] M. Thommes, K. Kaneko, A. V. Neimark, J. P. Olivier, F. Rodriguez-Reinoso, J. Rouquerol, and K. S. Sing, Pure and Applied Chemistry **87**, 1051 (2015).
[20] O. Glatter and O. Kratky, *Small angle X-ray scattering* (Academic press, 1982).
[21] G. A. Zickler, S. Jähnert, W. Wagermaier, S. S. Funari, G. H. Findenegg, and O. Paris, Physical Review B **73**, 184109 (2006).
[22] D. Zhao, J. Feng, Q. Huo, N. Melosh, G. H. Fredrickson, B. F. Chmelka, and G. D. Stucky, science **279**, 548 (1998).
[23] C. Lanczos, *The variational principles of mechanics* (Courier Corporation, 2012).
[24] B. Derjaguin and N. Churaev, Journal of Colloid and Interface Science **66**, 389 (1978).
[25] C. Pierce, The Journal of Physical Chemistry **64**, 1184 (1960).
[26] S. Gatica, M. Calbi, and M. Cole, Physical Review E **65**, 061605 (2002).
[27] M. W. Cole and W. Saam, Physical Review Letters **32**, 985 (1974).
[28] G. Findenegg, S. Groβ, and T. Michalski, in *Studies in Surface Science and Catalysis* (Elsevier, 1994), vol. 87, pp. 71–80.
[29] J. R. Philip, The Journal of Chemical Physics **67**, 1732 (1977).
[30] A. Silvestre-Albero, J. Silvestre-Albero, M. Martinez-Escandell, R. Futamura, T. Itoh, K. Kaneko, and F. Rodríguez-Reinoso, Carbon **66**, 699 (2014).

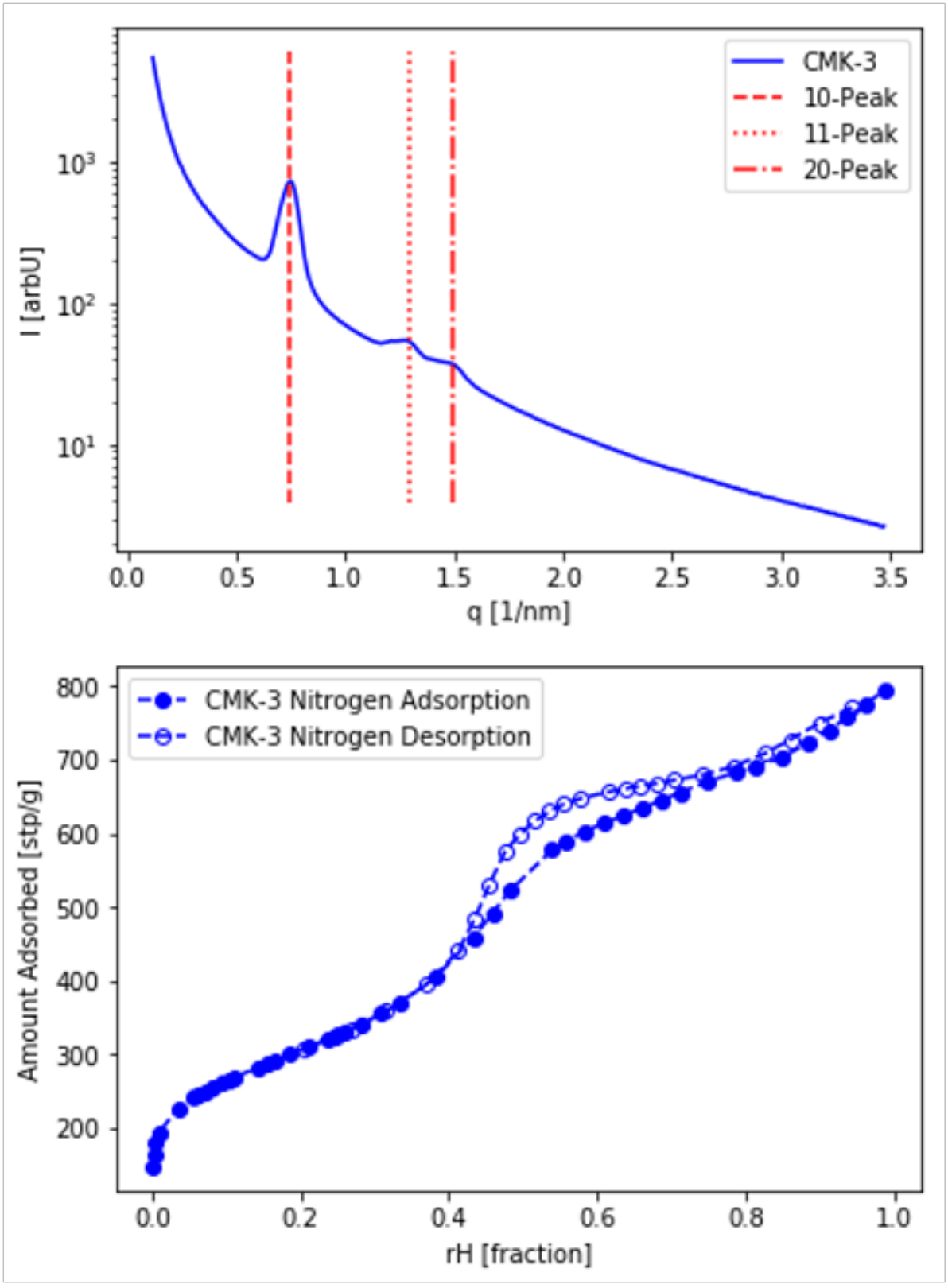

FIG. 2. a)The scattering curve of the CMK-3 material in this work. The (10),(11) and (20) peaks are highlighted. b) Ad- and desorption isotherm of the CMK-3 material in this work

.

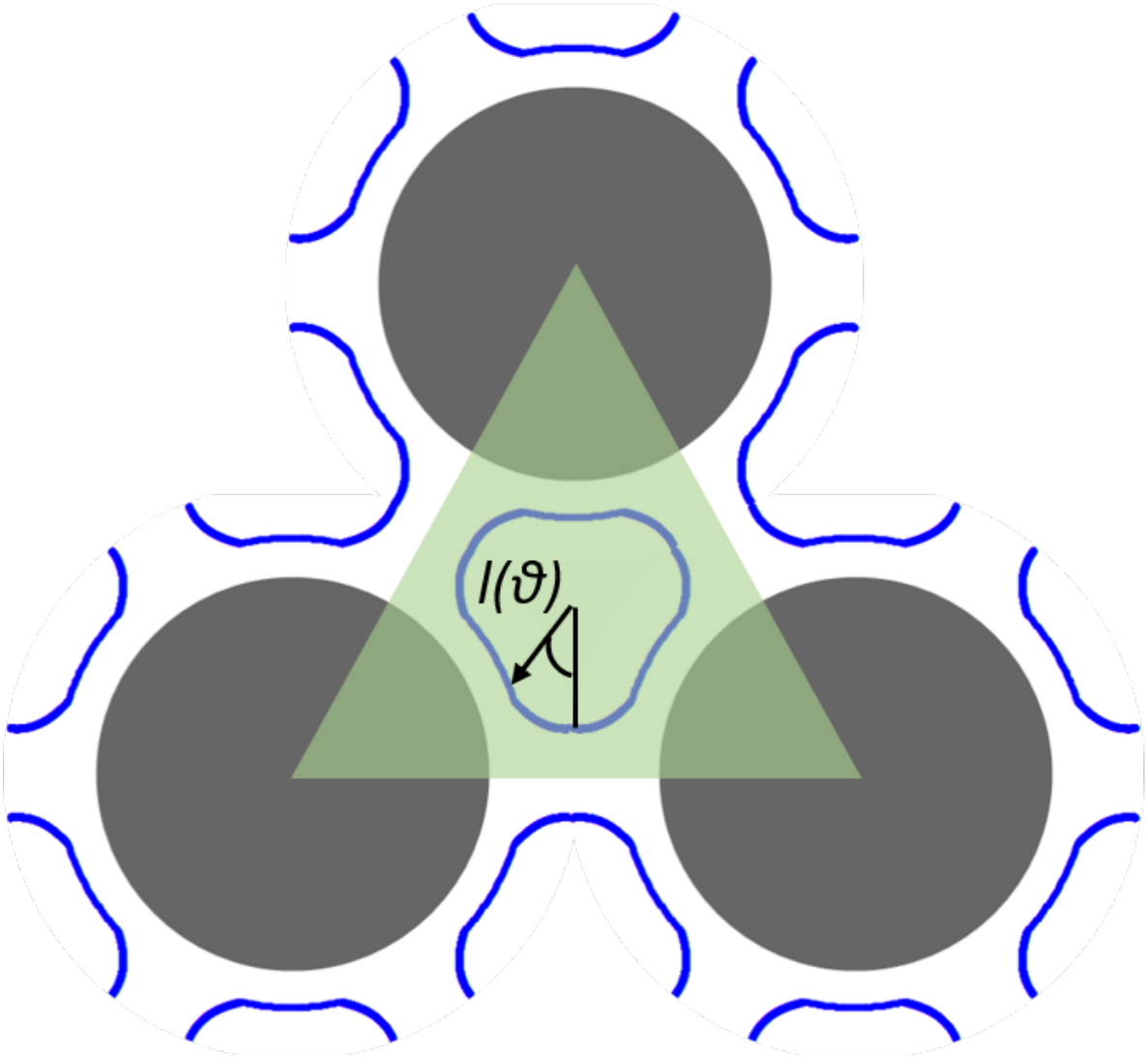

FIG. 3. A sketch of the geometric arrangement for a hexagonally ordered system of Carbon nanowires is depicted. $l(\Theta)$ describes the liquid vapour interface profile, the green triangle shows the unit cell in which we set the Grand Free Energy in equation 11

.

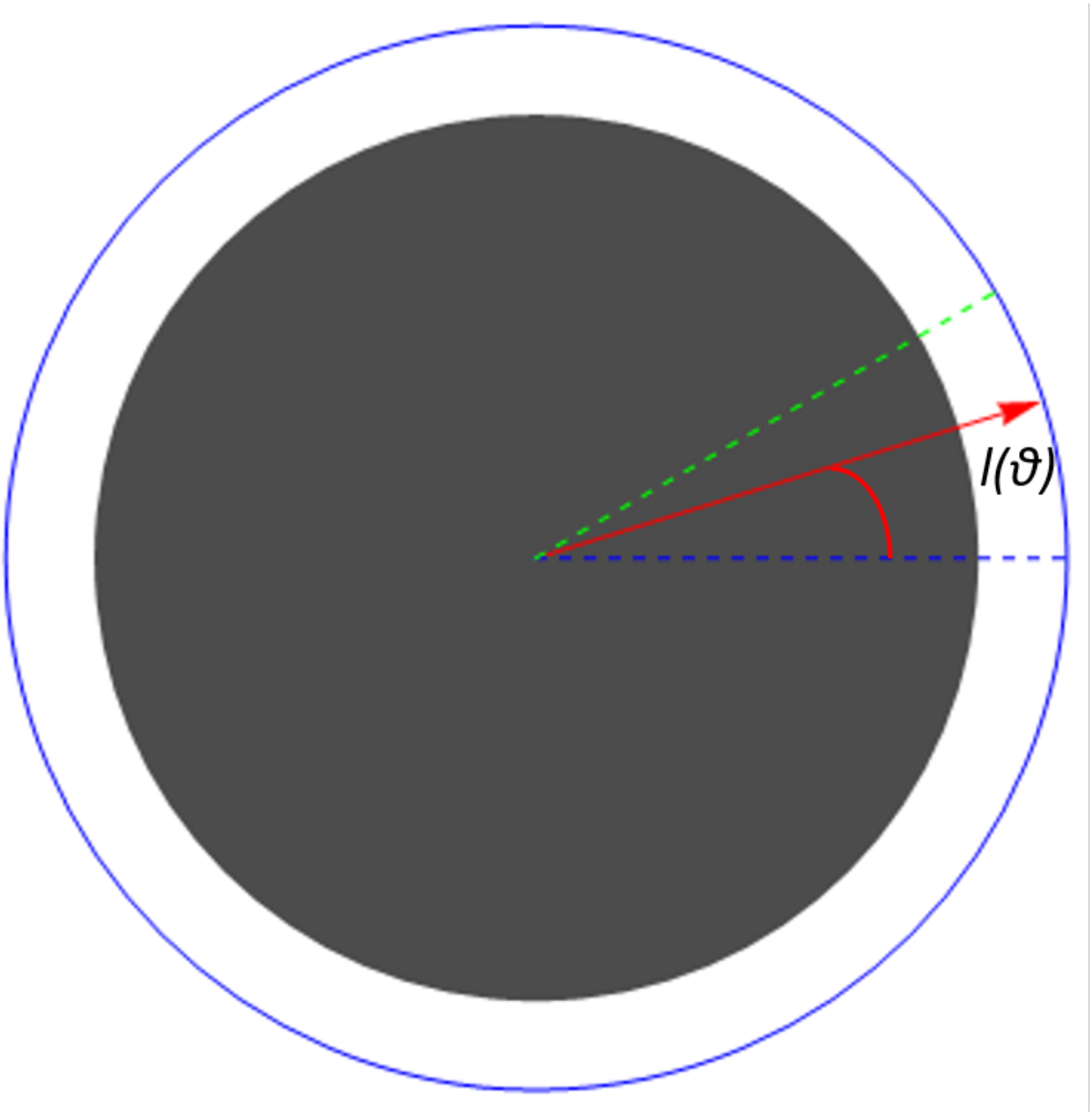

FIG. 4. The geometric relations to describe the layered solution to equation 27 are shown. The dashed green line indicates the maximal angle of integration $\frac{\pi}{6}$, the red arrow the liquid vapour interface profile vector $l(\Theta)$

.

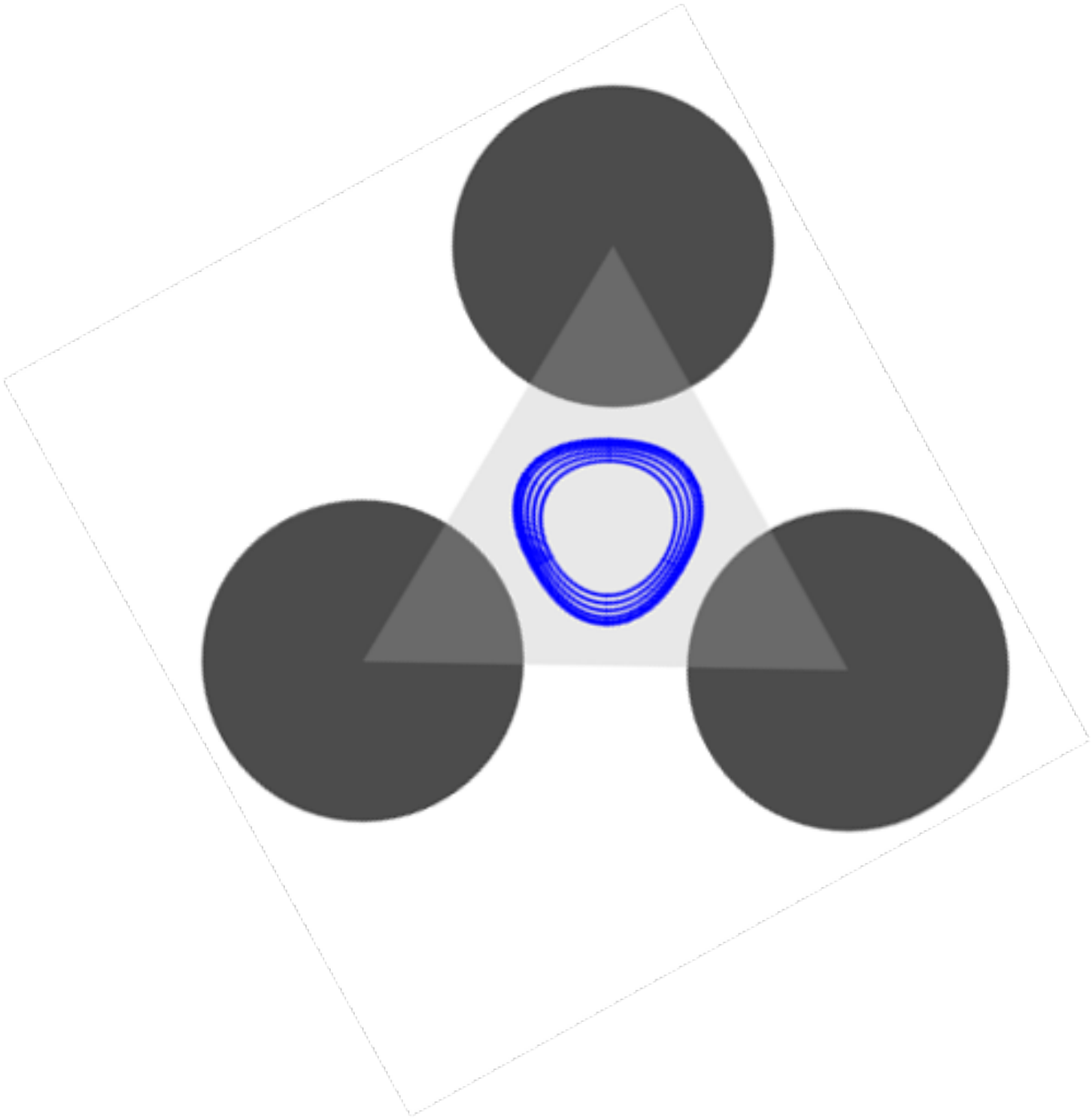

FIG. 5. Calculated profiles for the bridged phase in its relative pressure interval of existence are depicted. The unit cell in the material is highlighted by the triangle

.

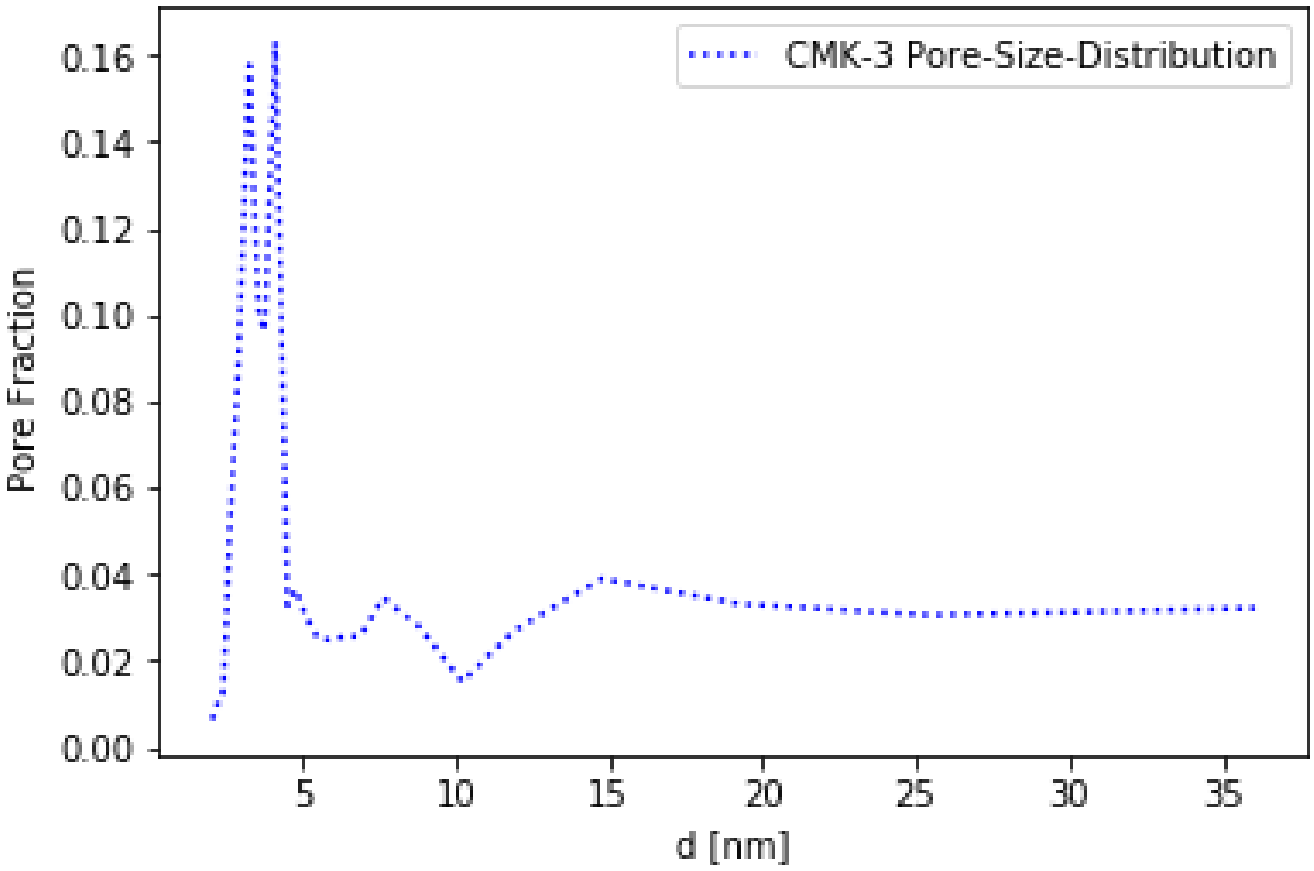

FIG. 6. The pore size distribution of the CMK-3 sample is depicted. The x-axis is displays the pore sizes and the y-axis the fractions of the according pore sizes.

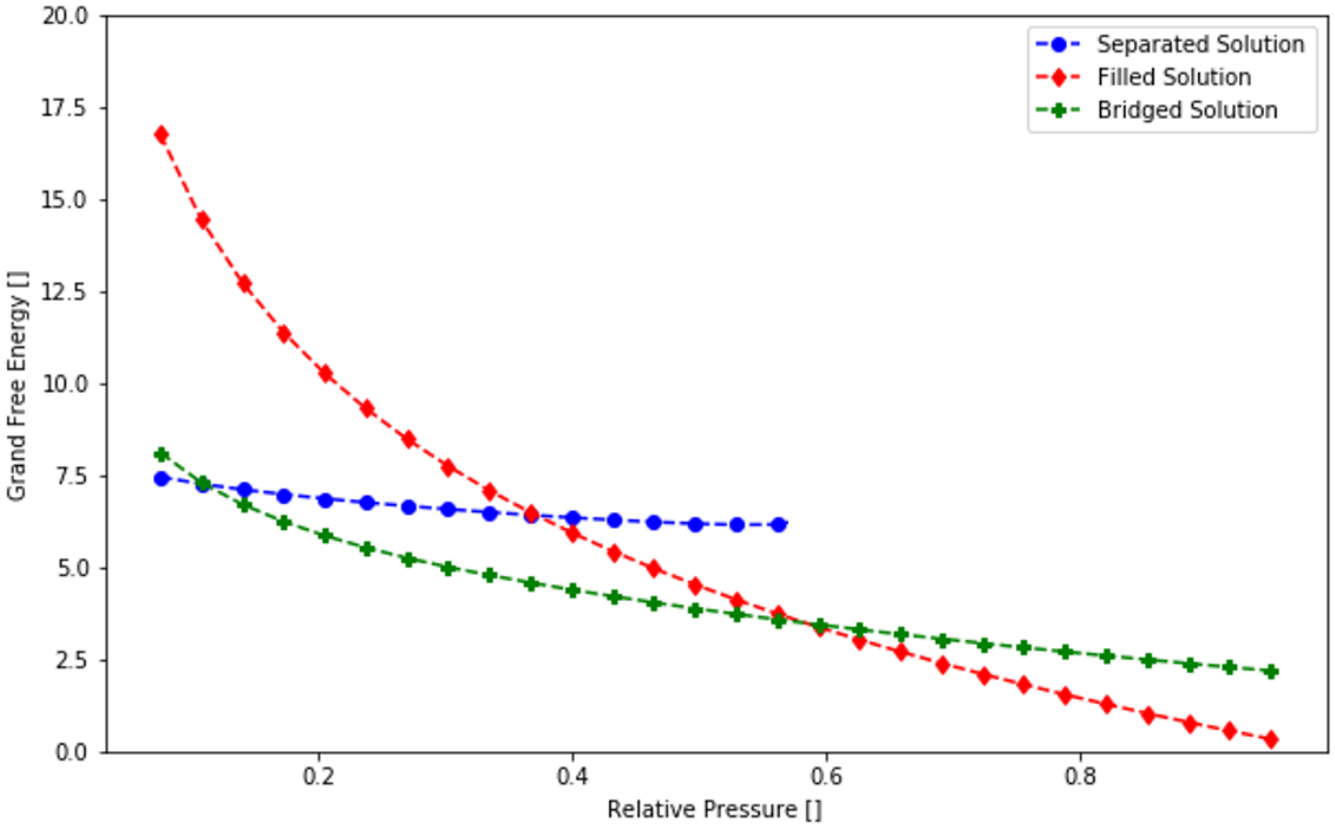

FIG. 7. Grand Free Energies as a function of the relative pressure for a system with a rod radius of 4.3 nm and a distance of 10.1 nm.

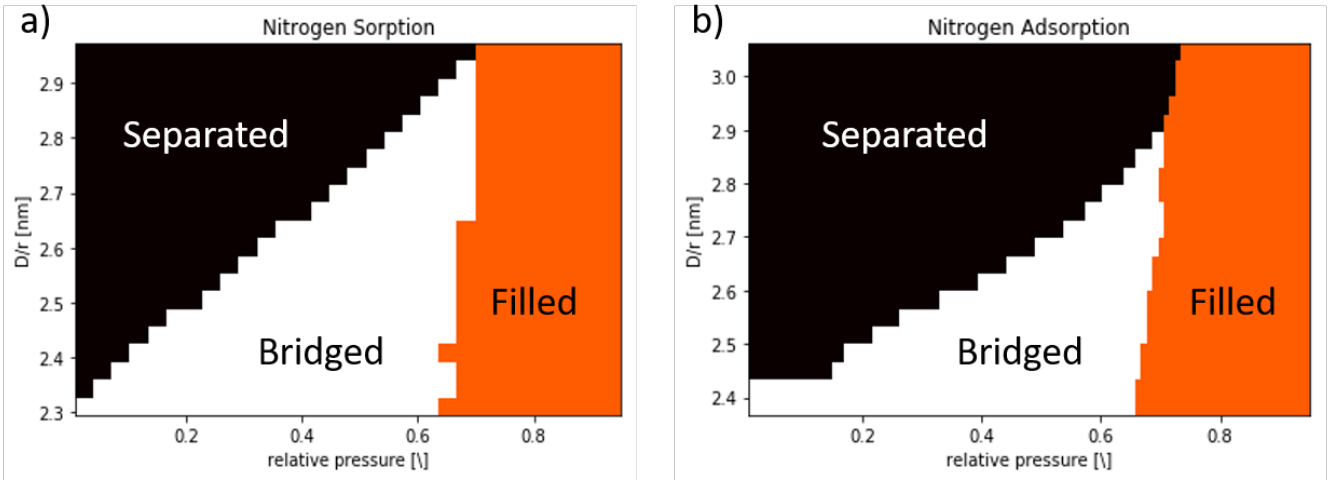

FIG. 8. The phase diagrams for Nitrogen adsorption on carbon are shown. a) Hexagonal arrangement of the carbon rods. b) Quadratic arrangement of carbon nanorwires.